ISSN 1453 – 7303 **"HIDRAULICA" (No. 2/2022)**
Magazine *of Hydraulics, Pneumatics, Tribology, Ecology, Sensorics, Mechatronics*

Numerical Simulation of Water Flow through an Ecological River Intake

Lect. **Ștefan-Mugur SIMIONESCU[1,*],** Assoc. Prof. **Daniela-Elena GOGOAȘE[1],**
Sci. Res. **Gabriela CÎRCIUMARU[2],** Sci. Res. **Rareș-Andrei CHIHAIA[2]**

[1] University Politehnica of Bucharest, Faculty of Energy Engineering, Department of Hydraulics, Hydraulic Machines and Environmental Engineering, 060042 Bucharest, Romania

[2] National Institute for R&D in Electrical Engineering ICPE-CA, 030138 Bucharest, Romania

* s.simionescu@upb.ro

Abstract: *The present study uses the CFD numerical approach to analyse the flow of water through the model of an ecological water intake structure located on the bank of a river. It aims to obtain and validate qualitative and quantitative hydrodynamic parameters, by comparing the numerical results with experimental data obtained previously on a small-scale model built in the laboratory. For this purpose, several numerical flow geometries with corresponding discretizations are specially built, under two simplifying assumptions: a 2D model, solved with HEC-RAS software and a 3D model, solved with the ANSYS Fluent code. Following the validation of the numerical results, the numerical model can be extended to a prototype of this ecological intake, which is to be built and located on a river in nature.*

Keywords: *River water intake, CFD simulation, HEC-RAS, ANSYS Fluent*

1. Introduction

Fish population and aquatic fauna decline represent indicators of environment degradation and alarms for human health. A negative impact on fish is related to the operation of river constructions for diversion, bypass, or intake of water. These constructions may be part of different complex facilities, such as: micro-hydropower developments – considered as a green energy source [1], irrigation pumping stations, water supply for household or industrial consumers, navigation, fish or touristic developments etc. If not properly designed, they may have a negative impact on the ecological flow, channel stability and survival of biota.

During operation of water intakes fish may pass through screens, into the feeder pipes or canals towards the turbines or other mechanical devices, or may remain on a river reach with insufficient water flow under improper surviving conditions. Protecting fish habitat around intakes or diversion constructions along the rivers represents a main interest for the engineers and scientific community [2], which have developed various physical or behavioural guiding systems to reduce entrainment of fish, such as: screens, bubble injection systems, noise, light, etc. Flow characteristics, such as temperature, velocity field or direction may attract or reject fish. However, few experimental investigations of the efficiency and impact of such systems exist.

Therefore, the main objective of the current study is to investigate through numerical simulations the flow through a previously designed ecological water intake, in order to obtain qualitative and quantitative information on the variation of characteristic hydrodynamic variables, important for the fish population. The validation of the numerical results is based on the experimental ones obtained on a laboratory model [3]. The results arising from the present numerical modelling can be applied in the case of a prototype of this ecological intake, which is to be built and located on a river in nature.

Numerical models based on Reynolds Averaged Navier-Stokes (RANS) equations compute the flow field by integrating the equations for conservation of mass (continuity) and conservation of momentum, the local equations of conservation of turbulent energy and, in case of two-phase systems, the equation of mass conservation for immiscible fluids [4]. As open channel flows through canals and rivers are turbulent, numerical simulations have been performed for this flow regime. Thus, the Navier-Stokes equation for laminar motion were averaged over time and added a turbulence closure, leading to the Reynolds averaged equations for turbulent motion (Reynolds Averaged Navier-Stokes equations - RANS, [5]).

2. Intake geometry

The ecological water intake model consists of a rectangular canal reach with a 1:1 H:V inclined bank and an another vertical one, with a smaller depth than the river channel, placed onto a river. In this bank are performed multiple orifices to collect the water (without suspended sediments) in a separate lateral chamber from which it is conducted into another canal or into a pipe [2]. Larger bedload sediments may be transported underneath this intake, on the riverbed. A variant of this intake may have a horizontal slit instead of orifices through which water can flow. This variant will be used in the present paper for the numerical simulations.

3. Methodology

The equation of conservation of mass for liquids, in differential form for 2 dimensions, is written:

$$\frac{\partial h}{\partial t} + \nabla \cdot (h\mathbf{v}) = q \quad (1)$$

where t - time, h - local water depth (from the free surface to the bed of the bed, vertical), q - lateral flowrate (may be positive in case of a lateral input/tributary or negative in case of an outlet).

The equation of conservation of momentum (motion) can be written (neglecting the Coriolis force effect) as follows:

$$\frac{\partial \mathbf{v}}{\partial t} + (\mathbf{v} \cdot \nabla)\mathbf{v} = -g\nabla z_s + \frac{1}{h}\nabla \cdot (\boldsymbol{\nu_t}\, h\, \nabla \mathbf{v}) - \frac{\boldsymbol{\tau_b}}{\rho R} + \frac{\boldsymbol{\tau_s}}{\rho h}, \quad (2)$$

where g is the gravitational acceleration, z_s is the free surface level with respect to an arbitrary reference level, $\boldsymbol{\nu_t}$ is the turbulent viscosity tensor with $\nu_{t,xx}$ and $\nu_{t,yy}$ being the coefficients of turbulent viscosity in the horizontal directions x and y, $\boldsymbol{\tau_b}$ is the tangential frictional force vector on the riverbed with its components $\tau_{b,x}$ and $\tau_{b,y}$, $\boldsymbol{\tau_s}$ is the tangential frictional force vector at the free surface due to wind, with its horizontal components $\tau_{s,x}$ and $\tau_{s,y}$ (usually neglected), R is the hydraulic radius. These equations are obtained from Reynolds equations for turbulent motion, which are mediated by depth.

The tangential viscous frictional force depends on the square of the velocity and on the coefficient of friction with the riverbed, C_f, which in turn can be expressed as a function of Manning's roughness coefficient, n, as follows [6-8]:

$$\boldsymbol{\tau_b} = \rho C_f |\mathbf{v}|\mathbf{v} = \rho \frac{n^2 g}{R^{1/3}} |\mathbf{v}|\mathbf{v}. \quad (3)$$

Since the Manning coefficient depends on the size of the bedrock sediment, vegetation, temperature, etc., it is usually initially estimated and then used as a calibration parameter for the numerical model.
The friction force due to the air is calculated with the relation:

$$\boldsymbol{\tau_s} = \rho_a C_D |\mathbf{w_{10}}|\mathbf{w_{10}}\,, \quad (4)$$

where is the density of air at sea level (≈ 1.29 kg/m^3), is the coefficient of friction at the surface of water with air and $\mathbf{w_{10}}$ is the air velocity at 10 m above the water.

The turbulent viscosity is calculated by the relation:

$$\boldsymbol{\nu_t} = \mathbf{D}\, u_*\, h + (C_s\Delta)^2 |\overline{S}|, \quad (5)$$

where $\mathbf{D}$ is the diffusion tensor (due to turbulence and dispersion), $u_* = \sqrt{\frac{\tau_b}{\rho}}$ is the rate of friction with the riverbed, C_s is the Smagorinsky coefficient (with values between 0.05 and 0.2), Δ is the size of the calculation mesh and $|\bar{S}|$ is the shear rate.

The system (1) - (5) has more unknowns than equations, so it must be completed with two more equations to quantify the turbulent efforts. As in the case of the RANS equations (from 3D modeling), several "closing" models are available for this, of which the most used are the $k-\varepsilon$ and $k-\omega$ models.
In the context of free surface flow on rivers, where the depth of the current is much smaller than the width of the river or the length of the computation reach, it is possible to simplify the equations of flow in 3 dimensions, by reducing them to two or even one dimension. Thus, the Shallow Waters Equations allow the following simplifying hypotheses [9], [10]:

- the fluid is incompressible (liquid), of uniform density;
- Reynolds equations are time-averaged so that the turbulent flow is approximated by the turbulent viscosity;
- the vertical scale is much smaller than the horizontal one, therefore, the vertical velocity is negligible and the vertical pressure distribution is hydrostatic.

Thus, the velocity vector $\mathbf{v}$ and the stresses in the mass and momentum conservation equations can only be written as a function of 2 components along the directions Ox (along the flow) and Oy (normal to it, in the direction of the banks), neglecting the component along Oz (of depth). The 2 components can be mediated in depth, on each calculation vertical, as follows [11-13]:

$$\begin{aligned} \mathbf{v} &= u\cdot\vec{\imath}+\mathrm{v}\cdot\vec{\jmath}\,; \\ u &= \frac{1}{h}\int_0^h u_s\,dz\,; \\ \mathrm{v} &= \frac{1}{h}\int_0^h \mathrm{v}_s\,dz\,, \end{aligned} \tag{6}$$

where u_s, v_s and h are the two local horizontal velocity components and depth, respectively.

3.1 Numerical simulation of the river intake model in 2D, with HEC-RAS

The HEC-RAS program solves the 2D equations of shallow water, especially for river flow, through a combination of methods of differences and finite volumes, on a computing unstructured polygonal network based on the finer topo-bathymetric subnetwork of the channel bottom below. Thus, the computational mesh consists in prismatic elements of vertical local depth. Each element volume is given by a relationship between the depth and base area. Since only one depth is calculated in the centre of each cell, it is important that the slope of the free surface and the velocity components do not vary greatly from one cell to another. Therefore, for the stability of the numerical models, computational networks with spatial steps as small as possible must be used. Hence the mesh is finer in the flow areas where there are large variations of the hydraulic parameters.

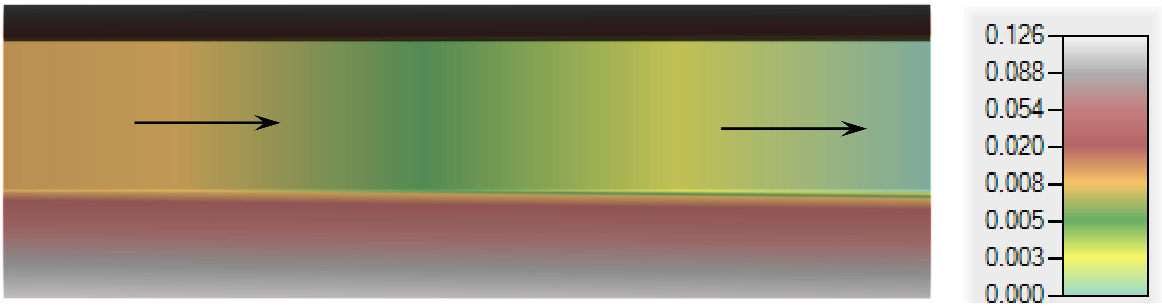

Fig. 1. Plane view of the canal with the elevations of the surface of the invert and the banks. The bank has a 1:1 H:V slope, on which the intake is located, is the lower one

For the 2D numerical study, the geometry characteristics are: main channel length L = 1 m and maximum width B = 0.3 m, was diagrammed in section with the left bank having the slope of H:V = 1:1 - as the experimental model, and the right bank at a slope H:V = 1:3 - unlike the experimental model which has a vertical wall. Then, starting from the cross-sections upstream and downstream, the 3D surface of the main channel was created, with an invert slope of 1%, i.e. 1 cm drop at 1 m length (Fig. 1).

It was not sought to reproduce the geometry of the experimental model identically, as the purpose of the 2D simulations was to obtain stable and fast results, only for preliminary qualitative field investigations.

For the 2D case, two more channel geometries were made (Fig. 2), as follows:

• G_1 - for the simple channel, without intake - for the initial verification of the hydraulic parameters;

• G_2 - for the intake channel, including a side sample with evenly distributed flow. It has been placed in the downstream part of the channel so that there is a sufficient length to stabilize the upstream profile.

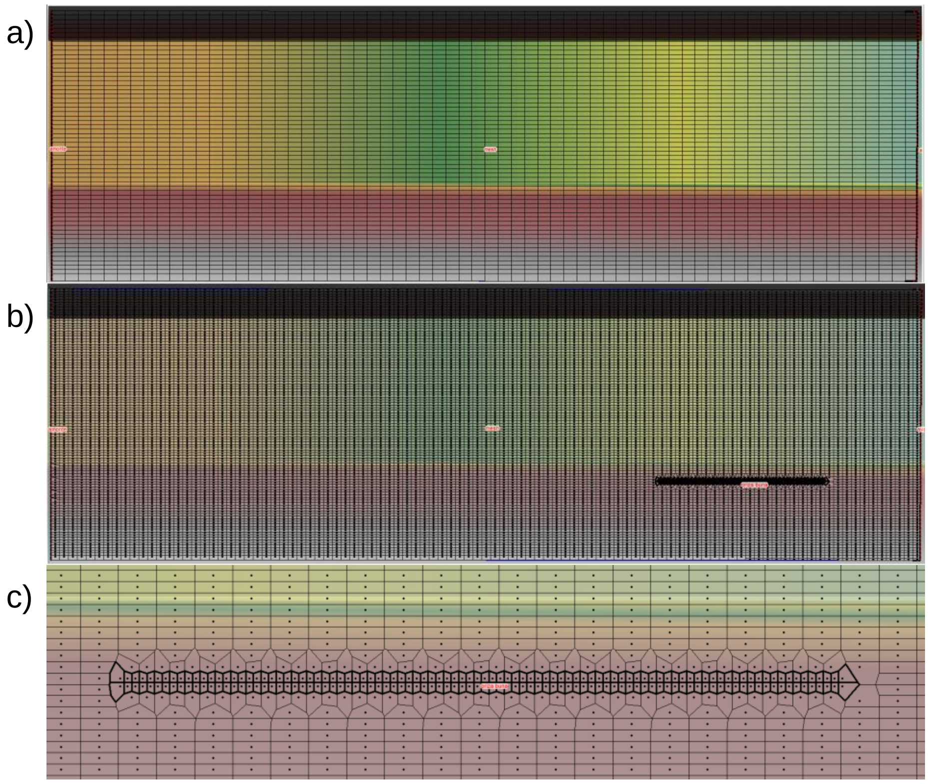

Fig. 2. Examples of 2D computational meshes for: (a) G_1 geometry with 4026 cells, b) G_2 geometry with 10296 cells, and c) detail at the intake of the calculation network for the schematization of the water sampling area at the outlet

For the G_1 geometry, the rectangular computation network (with regular-shaped cells) was created with several dimensions of the rectangular cell in the range 0.002 m - 0.01m, keeping the ratio between length and width the same as that of the channel ($L\!:\!B \approx \Delta x/\Delta y \approx 1\!:\!3$). This resulted in various discretization networks with a number of elements from 1000 to 15000. In the case of G_2 geometry, an irregular and finer network was created in the area of the intake. For the 2D case, the calculations were performed in an unsteady regime, but at a constant flow, and the imposed boundary conditions were:

- Upstream cross-section: flow rate of 5 l/s, corresponding to the experimentally measured velocity;

- Downstream cross-section: uniform regime condition with a slope equal to the slope of the main anal canal 1%;
- Laterally, at the intake - the flow taken through the intake, of 2 l/s (introduced as a negative input).

The simulations were performed with very small calculation steps, in the range of 0.1 ÷ 0.5 s over a period of 5 seconds, so as to stabilize the flow. Care was taken to comply with the Courant - Friedrich - Levy stability criterion (C <1, where C = v_calculation / v_flow) by either reducing the time step or the spatial step of the network to an acceptable limit.

3.2. Numerical simulation of the 3D Eco-WIBB experimental model with ANSYS Fluent

The numerical modelling of the free surface flow in the water intake was performed using the VOF method. In order to perform the numerical calculation with the help of the ANSYS Fluent code, geometries are constructed that reproduce the real flow domain. These domains are then discretized into finite elements of hexahedral volumes (quadrilateral prisms) and/or tetrahedrals/pentahedrals (triangular/quadrilateral pyramids), through a network of spatial discretization (mesh).

The construction of a geometry and the discretization of the flow field have a great influence on the obtained results. For the present study, the construction of the flow domain and its discretization were performed with the help of the ANSYS Gambit pre-processor. It offers a common set of CAD functions for domain creation, as well as specially implemented functions for creating complex, structured or unstructured discretization networks [15].

The geometry used to model the free surface flow corresponds to the actual geometry of the experimental laboratory installation: the upstream portion of the channel includes a long sector of l = 500 mm in the area where the main channel connection ramp is located. The length of the horizontal main channel is L = 1000 mm, of which l_p = 400 mm is the length of the water intake. The distance from the upstream section of the horizontal channel to the outlet was chosen so that the water speed could be stabilized, l_1 = 260 mm. The maximum height and the maximum width of the main channel were considered equal to those on the model, H_{max} = 117 mm, B = 280 mm, and the height of the lower tank h_{max} = 110 mm.

In order to obtain as clear results as possible on the studied flow, 3 three-dimensional flow geometries were built together with the related discretizations (Fig. 3):

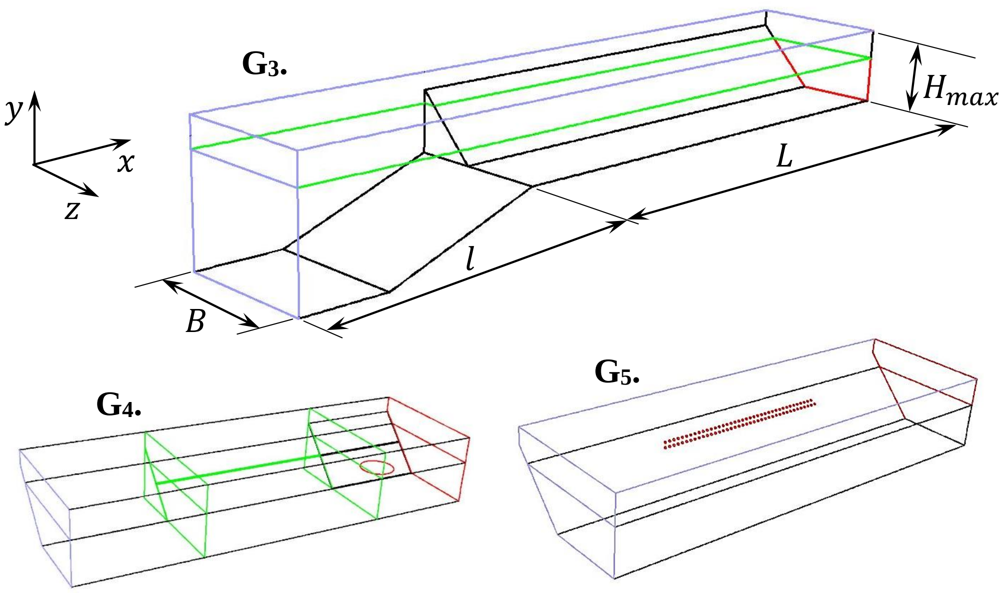

Fig. 3. Flow geometries built for 3D simulations; the definition of the coordinate system

- G_3 - preliminary, without water intake, for testing the flow parameters in the main channel. For this geometry, the upstream portion of the channel (l = 500 mm) was also considered, including the connecting ramp;
- G_4 - with simplified water intake in the form of a longitudinal slot, with an area equal to the area of the holes in the experimental model. To this geometry was added the lower tank for collecting water from the water intake;
- G_5 - complex, water intake with holes, similar to the experimental model.

The mesh dimensions for the geometries G_3, G_4 and G_5 are presented in Table 1.

Table 1: The characteristics of the discretization meshes for the 3 calculation geometries used

Geometry type	Nr. of cells	Nr. of faces	Nr. of nodes	Nr. of viscous layers at the walls	Mesh type	Type of mesh cells
G_3	1927748	5851616	1996632	3	unstructured	hexahedral
G_4	1297004	3715323	1158115	2	unstructured	hexahedral/pentahedral/ tetrahedral
G_5	2539809	5410914	680900	2	unstructured	hexahedral/pentahedral/ tetrahedral

The boundary conditions imposed for the 3D study are (Fig. 4): upstream main channel: water inlet speed (normal at the inlet surface) and constant water level (as the upstream section is far enough from the outlet, the speed distribution was imposed uniform [13]); downstream the main channel – atmospheric pressure; downstream – lateral to the water outlet of the intake chamber (G_4 and G_5) – atmospheric pressure.

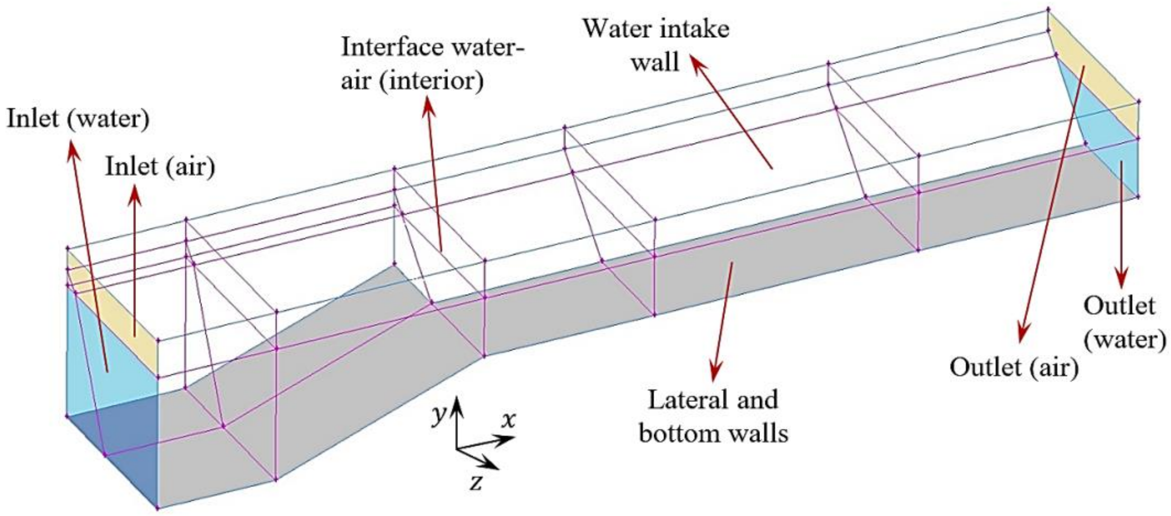

Fig. 4. Numerical calculation domain for G_3 geometry; boundary conditions imposed at the borders

4. Results and discussion

Figures 5 ÷ 8 show some qualitative results of the 2D simulations performed with the HEC-RAS program.

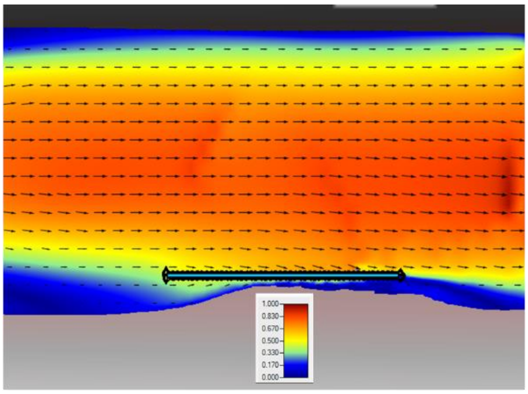

Fig. 5. Direction of velocity vectors for G_2 geometry near the intake

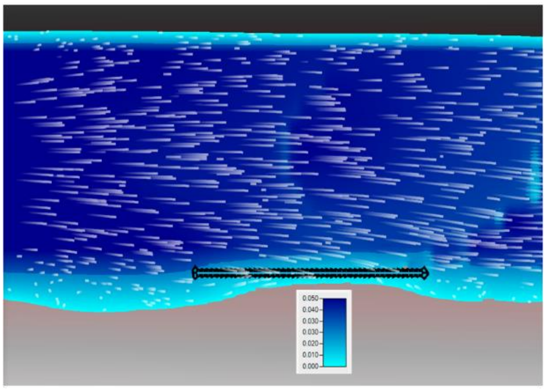

Fig. 6. Direction of streamlines for G_2 geometry in the intake area, superimposed over the water depth

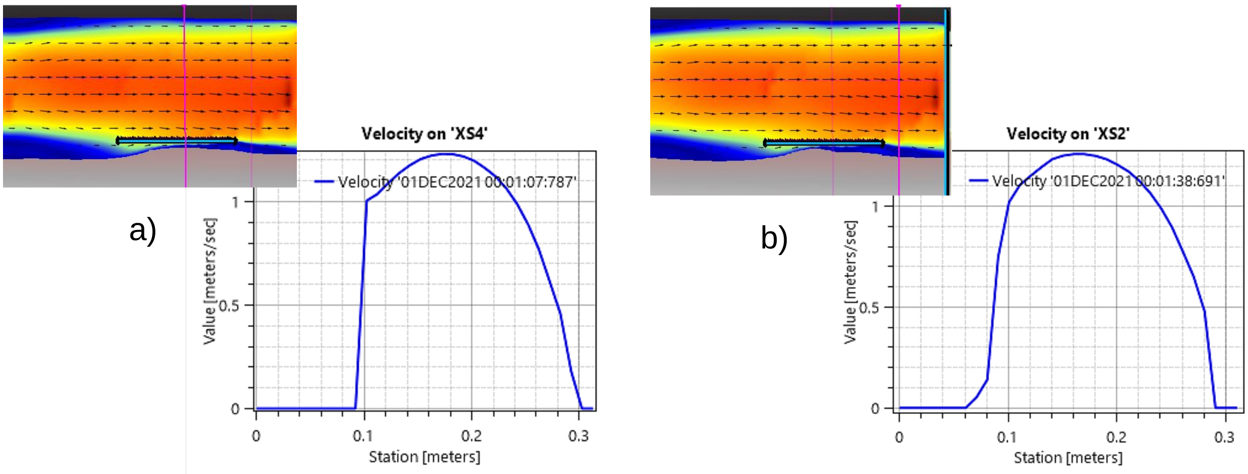

Fig. 7. The change in the shape of the velocity distribution for the G_2 geometry, in a cross section next to the intake (a) and downstream of it (b) (flow from the right)

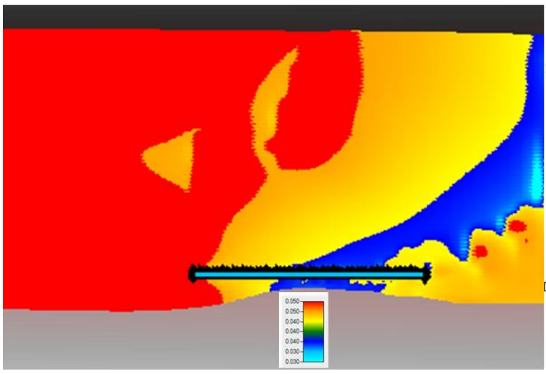

Fig. 8. The change (decrease) in the free surface area of the water near the intake for G_2 geometry

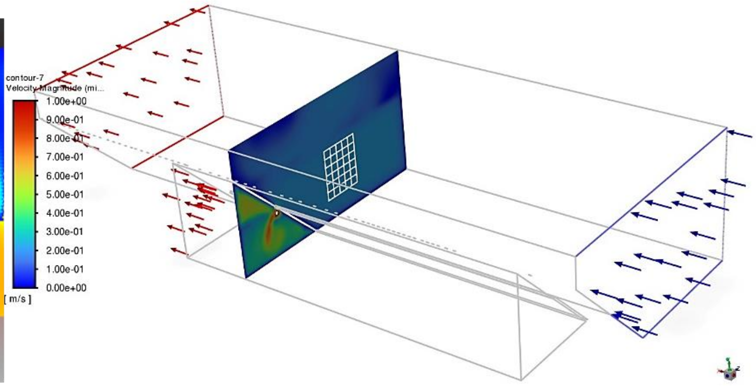

Fig. 9. Velocity distributions in a transversal measurement plane; position of the measurement lines for velocity distributions (G_4 geometry)

The results obtained from the 3D simulations are validated qualitatively and quantitatively based on the experimental results, for the average speeds of 0.22 m/s and 0.33 m/s. In this respect, in the numerical flow domain (geometry G_4) 6 vertical lines and 7 horizontal lines are created (Fig. 9) positioned similarly to the matrix for the experimental measurements with the Pitot-Prandtl tube. Figure 10 a) and b) show comparisons for validation between the numerical and experimental results, for the average velocity v = 0.22 m/s and, respectively, v = 0.33 m/s, on some of the vertical and horizontal lines of the test matrix. A good agreement was identified between the experimental and numerical results, both in terms of the value of the velocity and its trend.

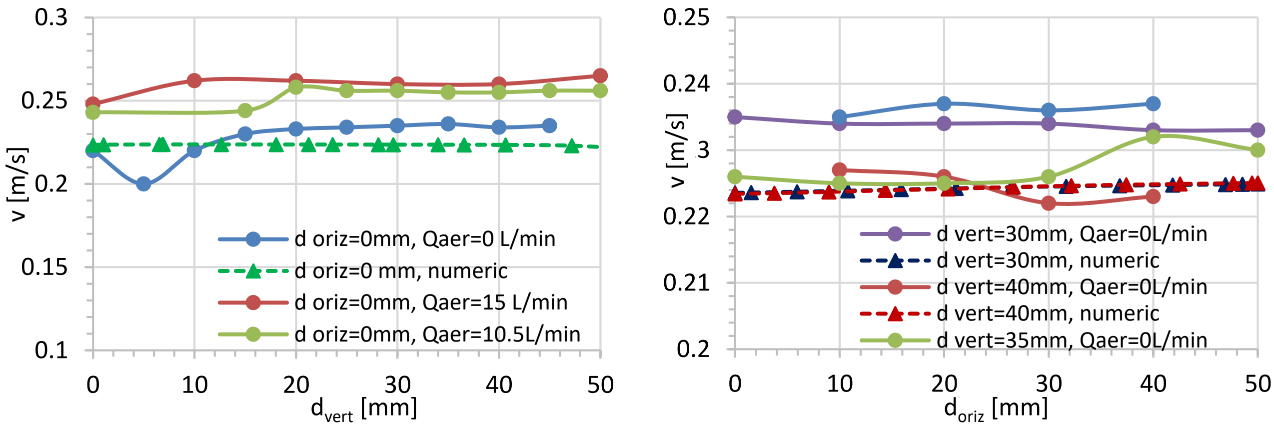

a) b)

Fig. 10. Comparison of numerical and experimental results, on vertical (a) horizontal (b) lines

Figure 11 shows velocity distributions in cross-section planes, for G_4 geometry. For better visibility of the flow area in the main channel, the velocity value scale has been adjusted so that areas with values between 0 and 1 m/s are visible. Figure 12 presents the velocity vectors in a horizontal plane at the water intake slot. They are dimensioned and coloured according to the value of the velocity and the area of water entry in the slot of the side outlet is observed.

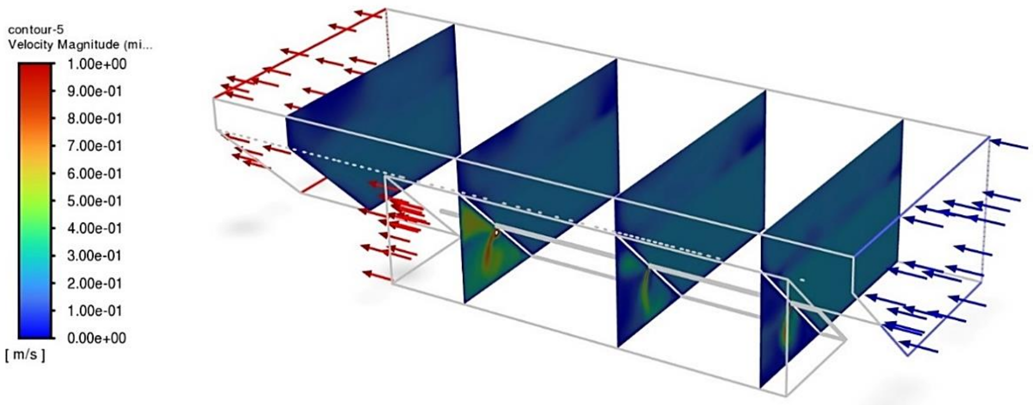

Fig. 11. Transversal velocity distributions for G_4 geometry

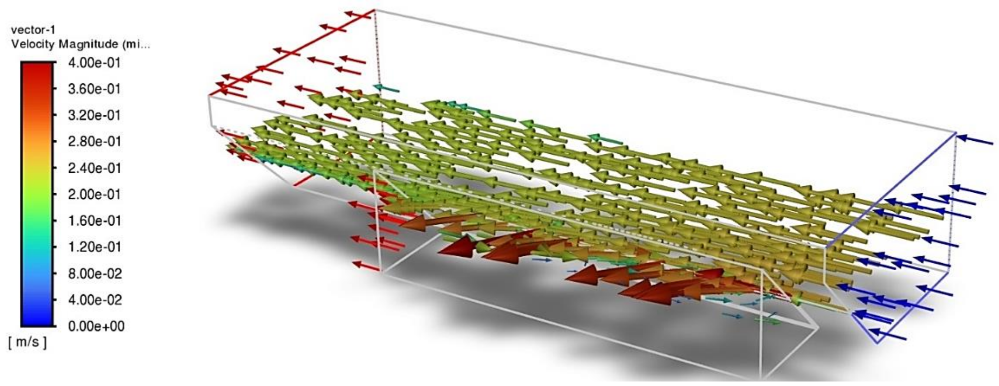

Fig. 12. Velocity vector distributions in a horizontal plane through the slit, colored by velocity, for G_4 geometry

The velocity distribution in a cross-section plane of the channel is shown in Figure 13. For better clarity in the flow area in the main channel, the velocity scale has been adjusted so that areas with values between 0 and 0.5 m/s are visible. At the median level of the water intake, the velocity distribution was extracted from the graph.

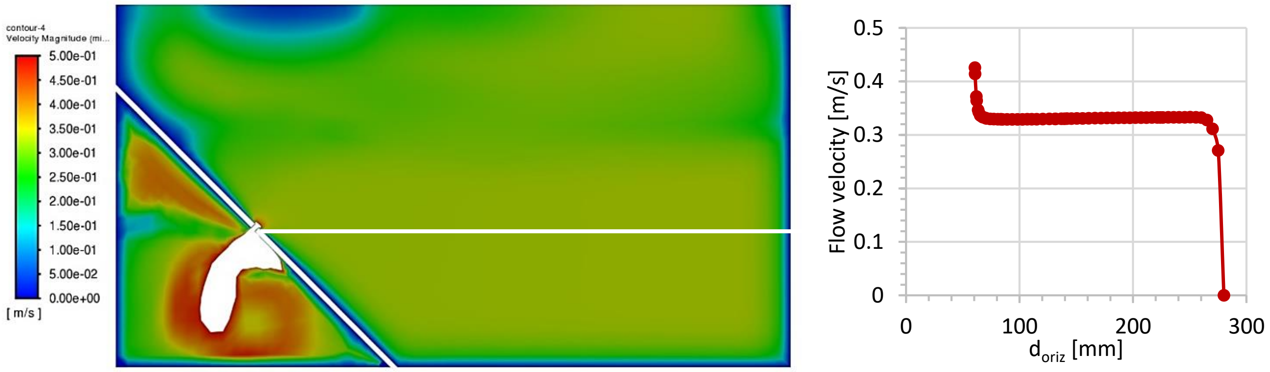

Fig. 13. Cross-section velocity distribution through channel and plot with velocity distribution at the water intake (horizontal line marked in white): horizontal distance is measured from left wall

Another quantitative criterion for comparing the numerical and experimental results is the balance of the inlet/outlet flows from the main channel, respectively from the water intake. The measured and numerically determined values are centralized in Table 2. For the first velocity at which experimental measurements and numerical simulations were made (v = 0.22 m/s), differences of 10.23% were obtained regarding the channel inlet flowrate, 7.61% for the outlet flowrate and 35.64% for the flow discharged through the water intake. For the second velocity at which experimental and numerical results were obtained (v = 0.33 m/s), there were differences of 5.2% in terms of channel input flowrate, 3.23% for channel output flowrate and 21.7% for the outlet discharged through the water intake. The differences in the main channel flowrates are fairly small, the higher relative errors for the water intake may be due to the constructive differences between the water intake holes on the physical model and the slot with equivalent area on the G_4 geometry in the simulations. In this sense, the numerical results on the G_5 geometry, which better reproduces the holes in the water intake, will be able to show an approximation of the experimental results.

Table 2: Balance of inlet / outlet flows in the water channel

Case	Water flowrate at the channel inlet (*l*/s)	Water flowrate at the channel outlet (*l*/s)	Water flowrate at the channel (*l*/s)	Inlet/outlet flowrate balance (*l*/s)
Exp., v = 0.22 m/s	4.23	-3.666	-0.564	–
Num., v = 0.22 m/s, G_4	4.663	-3.945	-0.765	-0.047
Exp., v = 0.33 m/s	6.345	-5.778	-0.567	–
Num., v = 0.33 m/s, G_4	6.676	-5.965	-0.690	0.021
Exp., v = 0.535 m/s	10.287	-9.72	-0.567	–

5. Conclusion

In the numerical simulations from this study, the calculation procedure was used to simulate the flow of water through an open channel with a water intake. Several sets of numerical simulations were performed on 2D and 3D geometries, in conditions similar to those tested experimentally on a laboratory model. The 2D simulations results offered a qualitative set of hydrodynamic variables of the flow field, whereas the 3D simulations were validated quantitatively based on the experimental results in the laboratory. Thus, the 3D simulations, could extend the experimental results to other points in the domain and other discharge value in the same range.

A challenge of the present study was the creation of 3D discretizations, taking into account the large dimensional differences of the working areas - for example, length 1000 mm, circular holes 4 mm. This has been overcome by the proper sizing of discretization meshes and the use of size functions. However, very fine discretizations led to very long computation time (> 24 h).

The velocity distribution resulting from the simulations shows a slight change in the intake area for the case of airless simulations. The longitudinal component of the velocity decreases to the detriment of the transversal one, which ensures the supply of water in the intake. For this reason, the level of the free surface also suffers a slight decrease in this area (a phenomenon qualitatively observed especially from the 2D simulations, performed at a ratio captured flow/transit flow ratio of 2/5, much higher than the one measured experimentally, 0.7/5).

Experimental measurements also showed a slight decrease in velocity towards the free surface near the outlet, but they could not detect the change in the local water depth, as the water flow captured by the intake was reintroduced into the channel, upstream. As the flow rate in the main channel was small, this disturbance has spread upstream, smoothing the level in the channel along its entire length.

In the future, an extension of the simulations on the G5 geometry is desired, as it reproduces best the water intake model tested in the laboratory, and also to perform the simulations in a biphasic system, including an air bubble curtain.

Acknowledgments

This work was funded by a grant of the Romanian National Authority for Scientific Research, CNCS, UEFISCDI, through the project PN-III-P2-2.1-PED-2019-1444, "Eco-hybrid water intake, with behavioural barrier to reduce the impact on fish fauna and river morphology – Eco-WIBB".

References

[1] Cowx, I. G., and M. Portocarrero Aya. "Paradigm shifts in fish conservation: moving to the ecosystem services concept." *Journal of Fish Biology* 79, no. 6 (December 2011): 1663-1680. https://doi.org/10.1111/j.1095-8649.2011.03144.x.
[2] Poletto, J. B., D. E. Cocherell, T. D. Mussen, A. Ercan, H. Bandeh, M. Levent Kavvas, J. J. Cech, and N. A. Fangue. "Fish-protection devices at unscreened water diversions can reduce entrainment: Evidence from behavioural laboratory investigations." *Conservation Physiology* 3, no. 1 (2015): 1–12. https://doi.org/10.1093/conphys/cov040.
[3] Cîrciumaru, G., R.-A. Chihaia, A. Voina, D.-E. Gogoașe Nistoran, Ș.-M. Simionescu, L.-A. El-Leathey, and L. Mândrea. "Experimental analysis of a fish guidance system for a river water intake." *Water* 14, no. 3 (2022): 370. https://doi.org/10.3390/w14030370.
[4] Versteeg, H. K., and W. Malalasekera. *An introduction to computational fluid dynamics. The finite volume method*. 1st edition. London, Longman Scie.&Tech., 1995.
[5] Shen, L., and E. S. Chan. "Numerical simulation of fluid–structure interaction using a combined volume of fluid and immersed boundary method." *Ocean Engineering* 35, no. 8 (June 2008): 939-952.
[6] Bălan, C. *Lectures in fluid mechanics / Lecţii de mecanica fluidelor*. Bucharest, Technical Publishing House, 2003.
[7] Jasak, H. *Turbulence Modelling for CFD*. Report for the NUMAP-FOAM Summer School, Zagreb, September 2-15, 2009.
[8] Pozrikidis, C. *Fluid dynamics: Theory, computation and numerical simulation*. 2nd edition. Springer, 2009.
[9] Moukalled, F., L. Mangani, and M. Darwish. *The Finite volume method in computational fluid dynamics. An Advanced Introduction with OpenFOAM® and Matlab*. Springer, 2016.
[10] Anderson, J.D. Jr., J. Degroote, G. Degrez, E. Dick, R. Grundmann, and J. Vierendeels. John F. Wendt (Ed.) *Computational Fluid Dynamics. An introduction*. 3rd edition. Springer, 2009.
[11] Rodriguez, S. *Applied Computational Fluid Dynamics and Turbulence Modeling. Practical tools, tips and techniques*. Springer, 2019.
[12] Blazek, J. *Computational Fluid Dynamics: Principles and Applications*. 3rd ed. Kidlington; Waltham, Elsevier, 2007.
[13] Bates, P., S. Lane, and R.I. Ferguson. *Computational fluid dynamics. Applications in Environmental Hydraulics*. John Wiley & Sons, 2005.
[14] ***. HEC-RAS 6.0 (2020), US Army Corps of Engineers, Hydraulic Engineering Center, River Analysis System, User's Manual.
[15] ***. Ansys Fluent 12 (2009) Tutorial 18. "Using the VOF Model".